

## Article

# Miniaturization of Anthracene-Containing Nonapeptides for Selective Precipitation/Recovery of Metallic Gold from Aqueous Solutions Containing Gold and Platinum Ions

Kin-ya Tomizaki <sup>1,2,\*</sup>, Tatsuki Tonoda <sup>1</sup>, Shungo Teramura <sup>1</sup>, Haruka Okazaki <sup>1</sup>, Takahito Imai <sup>1</sup> and Masahiro Asano <sup>3,\*</sup>

<sup>1</sup> Department of Materials Chemistry, Ryukoku University, Otsu 520-2194, Japan; tatsuki.tonoda.21@gmail.com (T.T.); T20M039@mail.ryukoku.ac.jp (S.T.); okakiyama0220@gmail.com (H.O.); imai@rins.ryukoku.ac.jp (T.I.)

<sup>2</sup> Innovative Materials and Processing Research Center, Ryukoku University, Otsu 520-2194, Japan

<sup>3</sup> Course of Environmental Ecological Engineering, Ryukoku University, Otsu 520-2194, Japan

\* Correspondence: tomizaki@rins.ryukoku.ac.jp (K.-y.T.); a02026@mail.ryukoku.ac.jp (M.A.); Tel.: +81-77-543-7469 (K.-y.T.); Fax: +81-77-453-7483 (K.-y.T.)

**Abstract:** The separation and recovery of noble metals is increasingly of interest, in particular the recovery of gold nanocrystals, which have applications in medicine and industry. Typically, metal recovery is performed using liquid–liquid extraction or electrowinning. However, it is necessary to develop noble metal recovery systems providing high selectivity in conjunction with a one-pot setup, ready product recovery, and the use of dilute aqueous solutions. In prior work, our group developed a selective gold recovery process using peptides. This previous research showed that RU065, a nonapeptide containing an anthracene moiety (at a concentration of  $2.0 \times 10^{-4}$  M), is capable of selective reduction of  $\text{HAuCl}_4$  to recover gold from a solution of  $\text{HAuCl}_4$  and  $\text{H}_2\text{PtCl}_6$ , each at  $5.0 \times 10^{-5}$  M. However, peptide molecules are generally costly to synthesize, and therefore it is important to determine the minimum required structural features to design non-peptide anthracene derivatives that could reduce operational costs. In this study, we used RU065 together with 23 of its fragment peptides and investigated the selective precipitation/recovery of metallic gold. RU065<sub>4–8</sub>, a fragment peptide comprising five amino acid residues (having two lysine, one L-isoleucine, and one L-alanine residue (representing six amide groups) along with an L-2-anthrylalanine residue) provided an Au/Pt atomic ratio of approximately 8, which was comparable to that for the full-length original RU065. The structural features identified in this study are expected to contribute to the design of non-peptide anthracene derivatives for low-cost, one-pot selective gold recovery.

**Keywords:** peptide; self-assembly; noble metal recovery; gold; platinum; anthracene



**Citation:** Tomizaki, K.-y.; Tonoda, T.; Teramura, S.; Okazaki, H.; Imai, T.; Asano, M. Miniaturization of Anthracene-Containing Nonapeptides for Selective Precipitation/Recovery of Metallic Gold from Aqueous Solutions Containing Gold and Platinum Ions. *Processes* **2021**, *9*, 2010. <https://doi.org/10.3390/pr9112010>

Academic Editor: Andrea Melchior

Received: 18 October 2021

Accepted: 8 November 2021

Published: 10 November 2021

**Publisher's Note:** MDPI stays neutral with regard to jurisdictional claims in published maps and institutional affiliations.



**Copyright:** © 2021 by the authors. Licensee MDPI, Basel, Switzerland. This article is an open access article distributed under the terms and conditions of the Creative Commons Attribution (CC BY) license (<https://creativecommons.org/licenses/by/4.0/>).

## 1. Introduction

The separation and recovery of noble metals from industrial wastewater has recently received significant attention as a component of sustainable chemistry. Especially, recovery of metals from electronic waste and other sources may be preferable to standard mining practices on a per mass basis, because discarded electronics contain greater relative proportions of metals compared with ores [1]. Meanwhile, it is also important to note that electronic waste tends to contain noble metals at relatively low levels mixed with other metals [2]. In order to separate metal ions of interest, liquid–liquid extraction is a common technique where metals such as gold and palladium can be extracted from an aqueous phase by employing specific organic solvents [3–7]. This technique is commonly used but is labor intensive and requires organic solvents that can have environmental impacts. In recent years, new approaches to liquid-based separation of noble metals have been demonstrated. These include the use of ionic liquids supported on silica to extract platinum group

metals [8] and the selective separation of gold by adsorption on polyhedral oligomeric silsesquioxanes tethered to imidazole thiones [9]. Metals can also be recovered via selective precipitation using electrowinning based on tuning electrode redox potentials, although this requires special instrumentation and produces hydrogen as a by-product under low metal ion concentrations [10,11]. An alternative approach for selective gold recovery is the use of sulfur atom-containing polymeric sorbents. For instance, 2,2'-thiobisethanol dimethacrylate was designed, synthesized, and demonstrated for selective gold separation under dilute conditions [12–14]. Selenium-containing polymers (polyselenoureas) were also synthesized and demonstrated for selective gold recovery [15]. Although there are now several excellent methods to selectively recover noble metals, especially gold, remaining requirements include (i) improvement of selectivity for specific metal elements, (ii) development of a simple one-pot processing method, (iii) development of a simple separation method for metals of interest, and (iv) development of an extraction method for homogenous, dilute water-based solutions.

Our own group has studied the synthesis of gold nanocrystals because this material exhibits special chemical and physical properties and is also biocompatible. Gold nanoparticles have applications as components of sensing or imaging devices, photonic or plasmonic systems, catalysts, and photothermal or drug delivery processes [16–24]. Previously, we demonstrated the formation of a nonapeptide capable of forming  $\beta$ -sheets (RU006: Ac-Ala-Ile-Ala-Lys-Ala-X-Lys-Ile-Ala-NH<sub>2</sub>, where X = L-2-naphthylalanine (Nal), Figure 1A). Combining HAuCl<sub>4</sub> with RU006 in water was found to fabricate gold nanoribbons having widths in the range of 50–100 nm, heights of several nanometers, and lengths below 1  $\mu$ m [25,26]. This process does not need additional reducing agents because the naphthalene moiety in the peptide can reduce HAuCl<sub>4</sub>. The formation of these nanoribbons is believed to proceed in several stages. Firstly, AuCl<sub>4</sub><sup>−</sup> ions are captured in the internal spaces of the peptide network based on electrostatic interactions with the L-lysine (Lys) side chains that form during self-assembly of the peptide. Following this, there is a transfer of electrons from the naphthalene groups to the Au(III) ions such that crystalline gold is gradually produced and gold nanoribbons are generated along the framework of the peptide by self-assembly. The obtained metallic gold-peptide composites are collected by simple centrifugation. Therefore, RU006 can be considered to act as a combination of an extracting agent, a reducing agent, and a precipitating agent during gold nanoribbon synthesis. Replacing the Nal group (which has a peak oxidation potential of 1.50 V) at the 6th position in the RU006 with an anthracene group (which has a stronger reducing effect and an oxidation potential of 1.05 V) to obtain [Ant<sup>6</sup>]-RU006 (X = L-2-anthrylalanine (Ant), referred to herein as RU065 (a), Figure 1B) has been found to form  $\beta$ -sheet conformation and modify the morphology of the resulting nanocrystals to generate spheres rather than ribbons [25,26].

Based on our prior results on the synthesis of gold nanocrystals using peptides containing aromatic side chains [25,26], we investigated the selective recovery of gold from homogenous aqueous (monophasic) solutions containing a mixture of dilute HAuCl<sub>4</sub> and H<sub>2</sub>PtCl<sub>6</sub> ( $5.0 \times 10^{-5}$  M each) using peptides ( $2.0 \times 10^{-4}$  M each) [27]. Much higher selectivity for gold (meaning Au-to-Pt (Au/Pt) atomic ratios of approximately 7.5) was obtained using the anthracene-containing peptide RU065 (a) than using the naphthalene-containing peptide RU006. The recovery of gold was confirmed by elemental analysis of precipitates obtained from the reaction mixtures after simple centrifugation. These precipitates likely resulted from the rapid reduction of the HAuCl<sub>4</sub> with the anthracene rings inhibiting electron reception by H<sub>2</sub>PtCl<sub>6</sub> [28,29]. On this basis, we concluded that anthracene-containing peptides could potentially be used to develop a selective gold precipitation/recovery process meeting the four criteria described above.



## 2. Materials and Methods

### 2.1. General

All solvents and reagents, unless otherwise noted, were purchased from Wako Pure Chemical Industries (Osaka, Japan) and used as received. The 9-fluorenylmethoxycarbonyl (Fmoc)-protected amino acid derivatives and reagents for peptide synthesis were purchased from Watanabe Chemical Industries (Hiroshima, Japan). Acetonitrile (high performance liquid chromatography (HPLC) grade) was purchased from Nacalai Tesque Inc. (Kyoto, Japan) and used for HPLC analysis and peptide purification. Ultrapure water (hereafter water) was purchased from Wako Pure Chemical Industries (Japan).

### 2.2. Peptide Synthesis and Storage

The original peptide RU065 (*a*) and its fragment peptides (*b–x*) were synthesized by performing Fmoc chemistry on Rink amide resin with 2-(1*H*-benzotriazole-1-yl)-1,1,3,3-tetramethyluronium hexafluorophosphate (HBTU) and 1-hydroxybenzotriazole monohydrate (HOBt·H<sub>2</sub>O) as coupling reagents [30]. The amino acid side chains of Lys groups were protected with *t*-butyloxycarbonyl (Boc).

Fmoc-protected Rink amide resin was treated with 20% piperidine (PPD) in *N*-methylpyrrolidone (NMP) (*v/v*) at room temperature for 15 min and washed with NMP three times to remove the Fmoc protecting groups. A solution of Fmoc-protected amino acid (10 eq), HBTU (10 eq), HOBt·H<sub>2</sub>O (10 eq), and *N,N*-diisopropylethylamine (DIEA, 20 eq) in NMP was added to a reaction vessel containing the N-terminal free Rink amide resin (1 eq), and the mixture was reacted at room temperature for 90 min for peptide chain elongation. The reaction mixture was filtrated and the resulting Fmoc-amino acid-bound resin was washed with NMP three times. The N-terminal Fmoc protecting groups of the resin were removed with 20% PPD /NMP (*v/v*) at room temperature for 15 min, and the resulting resin was washed with NMP three times. These coupling and deprotection cycles were repeated as required for peptide elongation. Subsequently, the Fmoc protecting groups at the N-termini of the peptide-bound resin were removed with 20% PPD/NMP (*v/v*) at room temperature for 15 min, and the resulting resin was washed with NMP three times. A solution of acetic anhydride (10 eq) and DIEA (10 eq) was added to the reaction vessel containing the N-terminal free peptide-bound resin (1 eq) and the mixture was reacted at room temperature for 30 min for N-terminal acetylation. The reaction mixture was filtrated and the resulting *N*-acetylated peptide-bound resin was washed with NMP three times, washed with chloroform three times, and then dried *in vacuo* to prepare a fully protected peptide-bound resin.

Final deprotection and cleavage of the resin-bound peptides were performed by treatment with trifluoroacetic acid (TFA)/thioanisole/*m*-cresol (90/7.5/2.5, *v/v/v*) at room temperature for 60 min. The reaction mixtures were concentrated and then precipitated with cold diethyl ether to provide the crude peptides. The crude peptides were washed with cold diethyl ether three times, dried *in vacuo*, and purified on a Hitachi LaChrom Elite HPLC system (Hitachi, Tokyo, Japan) using Cosmosil 5C<sub>18</sub>-AR-II packed columns (4.6 × 150 mm and 10 × 250 mm, Nacalai Tesque, Japan) with a linear gradient of acetonitrile/0.1% TFA, at a flow rate of 3.0 mL min<sup>-1</sup>. The purified peptides were lyophilized and characterized by MALDI-TOFMS (AXIMA-CFR Plus or MALDI-8020, Shimadzu, Kyoto, Japan).

Peptide stock solutions (*ca.* 1.0 × 10<sup>-3</sup> M) were prepared by dissolving each purified peptide powder in 2,2,2-trifluoroethanol (TFE) to prevent self-assembly during storage. The concentrations of the stock solutions of peptides (*a–x*) were determined by absorption spectroscopy (Shimadzu UV-3100 spectrophotometer, Japan) using an extinction coefficient of 5300 M<sup>-1</sup> cm<sup>-1</sup> at 377 nm for an Ant residue in methanol solutions containing 1% TFE (*v/v*) [27]. The peptide stock solutions were stored at −20 °C until use.

### 2.3. Preparation of Sample Solutions

According to a procedure previously described in the literature [27], a portion of each peptide stock solution in TFE was transferred to a microtube, dried with a N<sub>2</sub> gas stream,

then further dried *in vacuo* for 1 h. Water was added to the microtube to give a peptide concentration of  $4.0 \times 10^{-4}$  M and the solution was sonicated at 40 °C for 2 min to break up any peptide aggregates. Mixtures of equal volumes of the peptide solution and of an aqueous solution containing  $\text{HAuCl}_4$  and  $\text{H}_2\text{PtCl}_6$  (together with  $\text{Ni}(\text{NO}_3)_2$  if required;  $1.0 \times 10^{-4}$  M each) were incubated in a dry block heater (As One EB-303, As One, Osaka, Japan) at 40 °C for 24 h in the dark to prepare “sample solutions”.

#### 2.4. Absorption Spectra of Reaction Mixtures

A portion of each sample solution was transferred from the microtube to a 1.0 cm path length quartz cell and its UV–Vis absorption spectrum was recorded on a spectrophotometer (UV-3100, Shimadzu, Japan).

#### 2.5. Energy Dispersive X-ray Spectroscopy-Field Emission Scanning Electron Microscopy (EDS-FESEM)

According to a procedure previously described in the literature [27], a sample solution was centrifuged at 15,000 rpm (himac CT15E, Hitachi, Japan) for 3 min and the supernatant was removed. The resulting solid was redispersed in a small volume of water, and droplets of the suspension were applied to a transmission electron microscopy (TEM) grid (Cu 200 mesh covered with a collodion membrane, Nisshin EM, Japan), allowed to stand for 1 min, and dried with filter paper. The resulting sample was further dried *in vacuo* before acquiring images and performing an EDS analysis (JIB-4601F, JEOL, Akishima, Japan). The Au/Pt atomic ratio in the precipitate was calculated by comparing the intensities of the characteristic X-ray signals for gold and platinum obtained from 12 to 27 randomly selected areas per sample.

#### 2.6. Hydrophathy Assessment of Peptides by Reversed-Phase High-Performance Liquid Chromatography

According to a procedure described in the literature [31,32], 10  $\mu\text{L}$  aliquots of each peptide stock solution in TFE were analyzed by HPLC (LaChrom Elite HPLC system, Hitachi, Japan) using Cosmosil 5C<sub>18</sub>-AR-II packed columns ( $4.6 \times 150$  mm, Nacalai Tesque Inc., Japan) with a linear gradient from  $\text{H}_2\text{O}/0.1\%$  TFA to  $\text{CH}_3\text{CN}/0.1\%$  TFA over a span of 30 min, using a flow rate of  $1.0 \text{ mL min}^{-1}$  and UV detection at 220 nm. The retention times of the analytes were converted to relative hydrophobic index values ( $H$ ) using the equation:

$$H = 10 \times [t_R - t_R(\text{RU065}_{4-7}, p)] / [t_R(\text{RU065}_6, x) - t_R(\text{RU065}_{4-7}, p)] - 5.00 \quad (1)$$

where  $t_R$  is the retention time for the peptide of interest and  $t_R(\text{RU065}_{4-7}, p)$  and  $t_R(\text{RU065}_6, x)$  are the retention times for the most hydrophilic and hydrophobic peptides, respectively.

#### 2.7. Attenuated Total Reflection Fourier Transform Infrared (ATR-FTIR) Spectroscopy

According to a procedure previously described in the literature [25], an ATR-FTIR spectrum of peptide film prepared from a peptide solution obtained in the manner described above (peptide =  $1.0 \times 10^{-3}$  M in water, incubated at 40 °C for 24 h) was acquired on a Shimadzu Fourier transform infrared spectrophotometer IRTracer-100 (Japan) equipped with an ATR-8200HA unit (Shimadzu, Japan).

#### 2.8. Transmission Electron Microscopy

TEM samples were prepared using the procedure described above for the EDS-FESEM analyses and TEM images were acquired using a JEM-2100 instrument (JEOL, Japan) at an accelerating voltage of 200 kV.

#### 2.9. X-ray Diffraction (XRD)

The precipitates obtained after centrifugation of each sample solution were dried and mounted on a quartz sample cell. The XRD pattern was recorded on a RINT2000

spectrometer (Rigaku, Tokyo, Japan) with Cu-K $\alpha$  radiation with a scan area from 2.0 to 80.0°, a scan step of 0.02°, and a scan speed of 2.00° min<sup>-1</sup>.

### 2.10. Inductively Coupled Plasma-Optical Emission Spectroscopy (ICP-OES)

The supernatant (15 mL) obtained after centrifugation of each sample solution for 1 h at 15,000 rpm (himac CT15E, Hitachi, Japan) was analyzed by ICP-OES (Optima 5300DV, Perkin Elmer, Yokohama, Japan). The residual metal ion concentrations were calculated based on the working curves prepared by three-point-calibration using standard solutions of gold, platinum, and nickel.

## 3. Results and Discussion

**Design, Synthesis, and Characterization of the Peptides.** As described in the introduction, in prior work, our group synthesized [Ant<sup>6</sup>]-RU006, a nonapeptide forming amphiphilic  $\beta$ -sheets (referred to herein as RU065 (*a*)) and having the structure Ac-Ala-Ile-Ala-Lys-Ala-Ant-Lys-Ile-Ala-NH<sub>2</sub> (Figure 1B) [25,26]. The L-isoleucine (Ile) residues at the second and eighth positions in this peptide along with the Ant at the sixth position were all situated on the same side and so generated a hydrophobic face. A hydrophilic side was also produced based on the L-alanine (Ala) residues at the first, third, fifth, and ninth positions and the Lys at the seventh position, all of which were either less hydrophobic or, in the case of the Lys, were hydrophilic (see Figure 1B and Figure S1). A Lys residue was also present at the fourth position in proximity to the Ant on the hydrophobic side to allow interactions with AuCl<sub>4</sub><sup>-</sup> and PtCl<sub>6</sub><sup>2-</sup> ions, so as to both concentrate and reduce the metal ions in the self-assembled peptides to generate metallic precipitates. As noted, 23 different peptides having smaller structures than the original RU065 (that is, specimens *b*-*x*) were obtained by sequentially removing amino acid residues from both N- and C- termini to the Ant group at the sixth position of the original molecule. These fragment peptides are referred to herein as RU065<sub>*x-y*</sub>, where *x* and *y* are the positions on the original RU065 (*a*) at which these fragments begin and end, respectively (Figure 1C and Figure S1). As an example, RU065<sub>2-9</sub> (*b*) had the structure Ac-Ile-Ala-Lys-Ala-Ant-Lys-Ile-Ala-NH<sub>2</sub>, and so spanned the second to ninth positions of the original peptide, based on removing the Ala at the first position.

A typical solid-state peptide synthesis technique based on Fmoc chemistry was used to synthesize these peptides [30]. This synthesis was followed by purification using HPLC (Figure S2) and characterization by MALDI-TOFMS (Table S1 and Figure S2).

**Screening of Peptides by UV-Vis Absorption Spectroscopic Measurements.** We initially examined the abilities of peptides *a*-*x* to reduce the metal ions by preparing equivolume mixtures of aqueous peptide solutions (4.0 × 10<sup>-4</sup> M) and aqueous solutions containing HAuCl<sub>4</sub> and H<sub>2</sub>PtCl<sub>6</sub> (1.0 × 10<sup>-4</sup> M each) that were assessed using UV-Vis spectroscopy. Figure S3 shows the spectra of these sample solutions. It is evident that the majority of the peptide solutions (*a*-*u*) generated a surface plasmonic absorption band at approximately 540 nm, while the short fragments (*v*-*x*) produced a band at 580 nm. These results suggest the formation of spherical gold nanocrystals via the reduction of Au ions by the anthracene moieties in the former peptides (*a*-*u*), and also indicate that peptides (*v*-*x*) caused aggregation of the nanocrystals and/or provided anisotropic gold nanocrystals [25,33,34]. It should be noted that the formation of platinum nanocrystals could not be ascertained from the UV-Vis absorption spectra because this material did not generate characteristic peaks in the visible region of the spectrum [35].

**Screening of Peptides by EDS-FESEM Measurements.** We next separated the precipitates recovered from the sample solutions containing peptides (*a*-*x*), HAuCl<sub>4</sub>, and H<sub>2</sub>PtCl<sub>6</sub> following centrifugation and analyzed their morphologies and elemental distributions by EDS-FESEM. Figure S4 presents representative elemental mapping images of the precipitates for all peptides. In these images, the Au and Pt distributions are shown in yellow and purple, respectively, along with the corresponding EDS spectra. The results of replicate trials are summarized in Figure 2A. The Au/Pt atomic ratio for the precipitates

generated using the original RU065 (*a*) was  $8.4 \pm 0.4$ , while the fragment peptides lacking one, two, and three amino acids from the N-terminus of RU065 (*a*) (RU065<sub>*x*-9</sub> (*x* = 2–4, *b*–*d*)) all provided similar ratios of  $8.6 \pm 0.2$ ,  $8.6 \pm 0.6$ , and  $8.8 \pm 0.5$ , respectively. Surprisingly, the deletion of four and five amino acids from the N-terminus of the RU065 (peptides *e* and *f*) gave much lower ratios of  $4.9 \pm 0.3$  and  $5.1 \pm 0.6$ , respectively.

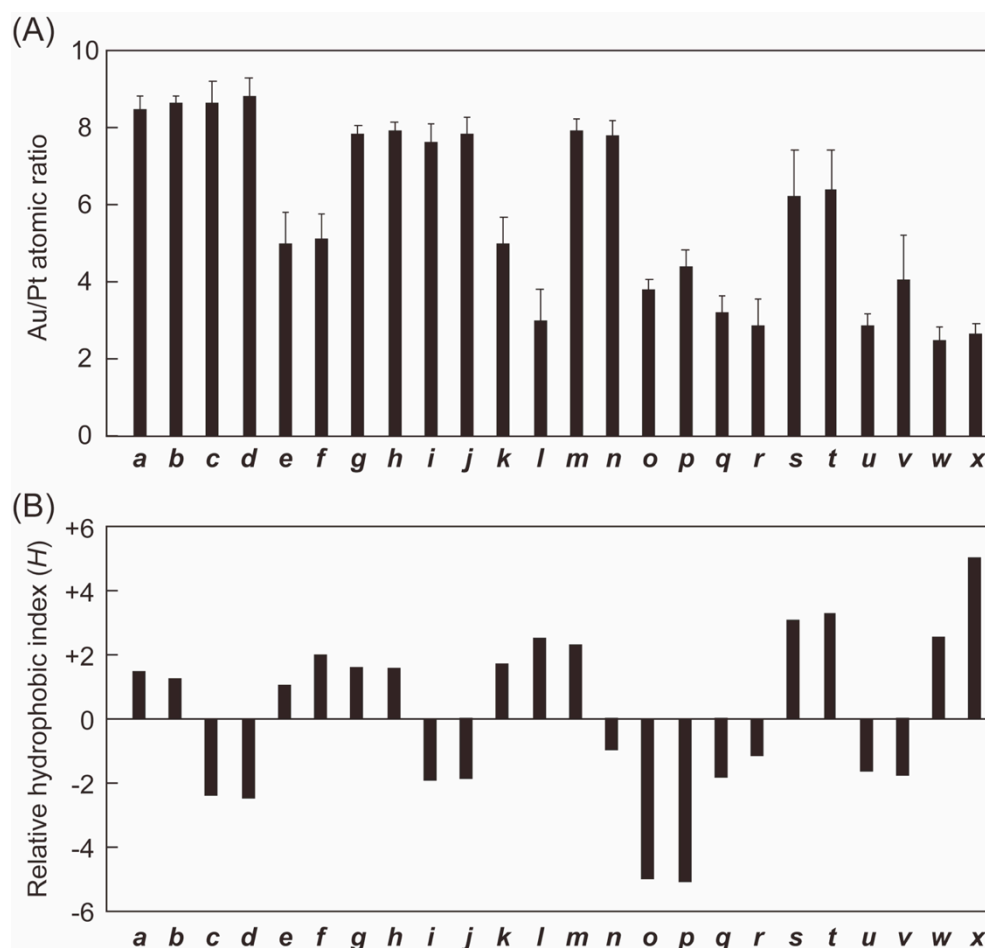


**Figure 2.** (A) Au-to-Pt (Au/Pt) atomic ratios for precipitates obtained from mixtures of HAuCl<sub>4</sub>, H<sub>2</sub>PtCl<sub>6</sub> and peptides *a*–*x* as determined by EDS-FESEM analyses of randomly selected areas (mean  $\pm$  SD, *n* = 12–27). Peptide =  $2.0 \times 10^{-4}$  M, HAuCl<sub>4</sub> = H<sub>2</sub>PtCl<sub>6</sub> =  $5.0 \times 10^{-5}$  M in water. Reactions were conducted at 40 °C for 24 h in the dark. (B) Relative hydrophobic index (*H*) values for peptides *a*–*x* as determined by reverse-phase HPLC. Positive and negative values indicate hydrophobic and hydrophilic materials, respectively.

We also examined the series of fragment peptides lacking an Ala residue at the ninth position of the RU065 (*a*) (RU065<sub>*x*-8</sub> (*x* = 1–6, *g*–*l*)) and found that the deletion of one, two, and three amino acids from the N-terminus of RU065<sub>1-8</sub> (*g*) provided excellent gold selectivity, with ratios of  $7.8 \pm 0.2$  (RU065<sub>1-8</sub> (*g*)),  $7.9 \pm 0.2$  (RU065<sub>2-8</sub> (*h*)),  $7.6 \pm 0.5$  (RU065<sub>3-8</sub> (*i*)) and  $7.8 \pm 0.4$  (RU065<sub>4-8</sub> (*j*)), respectively. These values were comparable to those for peptides *a*–*d*. In contrast, greatly decreased Au/Pt atomic ratios of  $5.0 \pm 0.7$  and  $3.0 \pm 0.8$  were determined for RU065<sub>5-8</sub> (*k*) and RU065<sub>6-8</sub> (*l*), respectively. These observations strongly indicate that the Lys residue at the fourth position of the original RU065 (*a*) was important with regard to obtaining significant gold selectivity.

The fragment series RU065<sub>*x*-7</sub> (*x* = 1–6, *m*–*r*), lacking two amino acid residues at the eighth and ninth position of the original RU065 (*a*), were also assessed by EDS-FESEM. RU065<sub>1-7</sub> (*m*) and RU065<sub>2-7</sub> (*n*) provided suitable levels of selectivity, with ratios of  $7.9 \pm 0.3$  and  $7.8 \pm 0.4$ , respectively. However, the deletion of the Ile residue at the second

position of RU065<sub>1-7</sub> (*m*) afforded significantly decreased Au/Pt ratios of  $3.8 \pm 0.3$  and  $4.3 \pm 0.5$  in the case of the RU065<sub>3-7</sub> (*o*) and RU065<sub>4-7</sub> (*p*), respectively. The RU065<sub>*x-7*</sub> (*x* = 5–6, *q–r*) specimens did not provide large variations in the ratio even though the Lys residue at the fourth position was deleted in both, with RU065<sub>5-7</sub> (*q*) and RU065<sub>6-7</sub> (*r*) giving ratios of  $3.2 \pm 0.4$  and  $2.8 \pm 0.7$ , respectively. These data suggest that the presence of a hydrophobic Ile residue at the second position of RU065<sub>1-7</sub> (*m*) was vital to realizing high selectivity for gold. This effect is attributed to the lack of hydrophobic Ile and Ala residues at the eighth and ninth positions of the original RU065 (*a*) in the RU065<sub>*x-7*</sub> (*x* = 1–6, *m–r*) fragments.

Lastly, we examined the selectivity of the RU065<sub>*x-6*</sub> (*x* = 1–5, *s–w*) specimens, which lacked three amino acid residues at the seventh, eighth, and ninth positions of the original RU065 (*a*), and of Ac-Ant-NH<sub>2</sub> (RU065<sub>6</sub> (*x*)), which comprised only an Ant residue. The selectivity data trend for these peptides was similar to that for the RU065<sub>*x-7*</sub> (*x* = 1–6, *m–r*) series. That is, the ratios for RU065<sub>1-6</sub> (*s*) and RU065<sub>2-6</sub> (*t*) showed slightly reduced values of  $6.2 \pm 1.2$  and  $6.4 \pm 1.0$ , respectively, compared with those for peptides *a–d*, *g–j*, *m*, and *n*. The removal of the Ile residue at the second position of RU065<sub>1-6</sub> (*s*) evidently lowered the ratio, giving values of  $2.8 \pm 0.3$ ,  $4.0 \pm 1.2$ ,  $2.5 \pm 0.4$ , and  $2.6 \pm 0.3$  for the RU065<sub>*x-6*</sub> (*x* = 3–5, *u–w*) and RU065<sub>6</sub> (*x*) fragments, respectively. From these data, it appears that the incorporation of a hydrophobic Ile residue and a positively charged Lys residue is necessary for good selectivity. This is likely because the Ile and Lys residues facilitate the initial self-assembly of the peptide through hydrophobic interactions and also promote the accommodation/enrichment of AuCl<sub>4</sub><sup>−</sup> ions within the self-assembled peptide nanostructure, based on the proposed mechanism [25,26].

**Hydropathy Assessment.** The EDS-FESEM experiments described above highlighted the importance of characterizing the hydropathy of the original RU065 (*a*) and its fragment peptides (*b–x*) by HPLC analysis [31,32]. Figure 2B summarizes the *H* values for these specimens. Note that more positive values are associated with more hydrophobic compounds while negative values indicate more hydrophilic species. These data demonstrate that the original RU065 (*a*) was relatively hydrophobic but a significant transition from hydrophobic to hydrophilic was induced by removing the hydrophobic Ile residue at the second position between RU065<sub>2-9</sub> (*b*) and RU065<sub>3-9</sub> (*c*). The deletion of the hydrophilic Lys residue at the fourth position led to another significant transition from hydrophilic back to hydrophobic between RU065<sub>4-9</sub> (*d*) and RU065<sub>5-9</sub>. Similar transitions also occurred between RU065<sub>2-8</sub> (*h*) and RU065<sub>3-8</sub> (*i*) and between RU065<sub>4-8</sub> (*j*) and RU065<sub>5-8</sub> (*k*). In the case of the RU065<sub>*x-7*</sub> (*x* = 1–6, *m–r*) series, there was a change from hydrophobic to hydrophilic following the removal of the hydrophobic Ile residue at the second position on going from RU065<sub>2-7</sub> (*n*) to RU065<sub>3-7</sub> (*o*), resulting in the most hydrophilic peptide lacking two hydrophobic Ile residues at the second and eighth positions. Although the deletion of the Lys at the fourth position to generate RU065<sub>5-7</sub> (*q*) decreased the relative hydrophilicity of this peptide (or more accurately increased the relative hydrophobicity), its *H* value was still within the hydrophilic range because it did not have two of the Ile residues. The *H* values for the RU065<sub>*x-6*</sub> (*x* = 1–5, *s–w*) series and RU065<sub>6</sub> (*x*) also demonstrated a significant transition from hydrophobic to hydrophilic between RU065<sub>2-6</sub> (*t*) and RU065<sub>3-6</sub> (*u*) and from hydrophilic to hydrophobic between RU065<sub>4-6</sub> (*v*) and RU065<sub>5-6</sub> (*w*). These transitions were similar to those that occurred in the other series. The most hydrophobic fragment was RU065<sub>6</sub> (*x*), which contained only one Ant residue. The smaller peptide structures afforded higher *H* values, likely due to the greater contributions of individual amino acid residues.

**Determination of Miniaturized Active Structures.** The relationship between the Au/Pt atomic ratios determined from Figure 2A and the *H* values from Figure 2B for all peptides, along with the amino acid residues comprising each specimen, are presented in Figure 3. Those fragments having *H* values between −2 and +2 provided the best ratios (in the vicinity of 8). Specifically, these specimens were *a*, *b*, *c*, *d*, *g*, *h*, *i*, *j*, *m*, and *n*, among which the smallest peptide was RU065<sub>4-8</sub> (*j*), having five amino acid residues including two Lys and one Ile (Figure 4A). On this basis, we determined that RU065<sub>4-8</sub> (*j*)

had the minimum structure required to precipitate/recover gold from a mixture of gold and platinum ions.

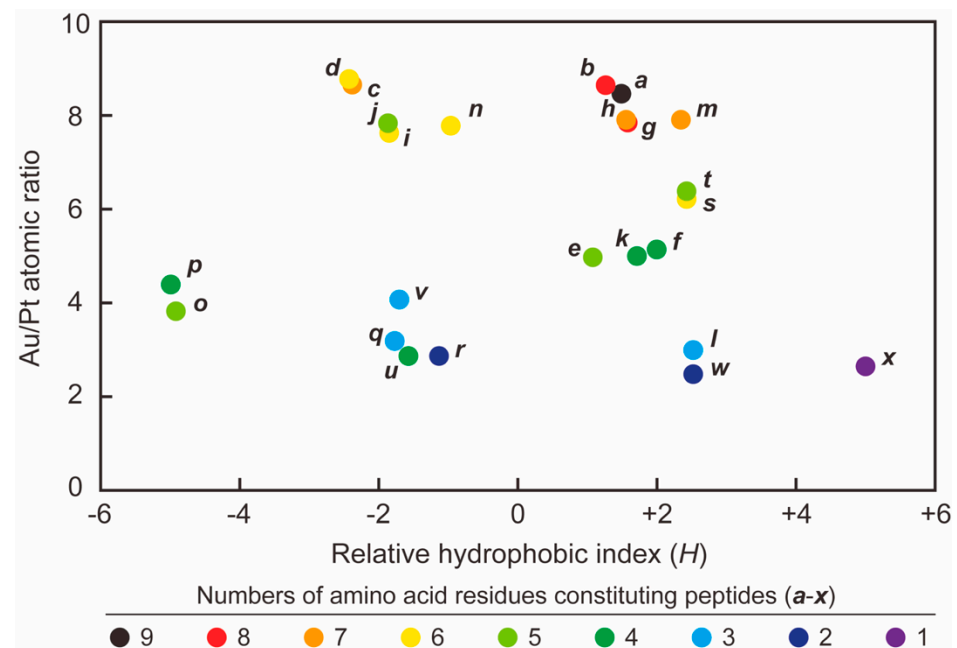


**Figure 3.** Relationships between the relative hydrophobic indices ( $H$ ) for peptides  $a-x$ , the Au/Pt atomic ratios for the precipitates obtained with those peptides, and the number of amino acids constituting the peptides. These data are taken from Figure 2.

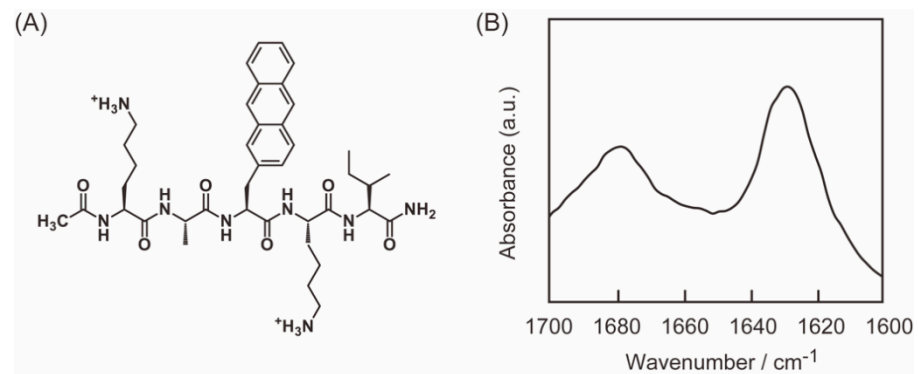


**Figure 4.** (A) Molecular structure of RU065<sub>4-8</sub> ( $j$ ), a peptide fragment with the potential to selectively recover Au from mixtures of Au and Pt ions. (B) ATR-FTIR spectrum of RU065<sub>4-8</sub> ( $j$ ) peptide film prepared from an aqueous solution (peptide =  $1.0 \times 10^{-3}$  M, incubated at 40 °C for 24 h).

Next, we characterized the secondary structure of the miniaturized active peptide RU065<sub>4-8</sub> ( $j$ ) by measuring the ATR-FTIR spectrum of a peptide film prepared from aqueous solution (Figure 4B). The amide I region, originating from the amide carbonyl stretching frequencies between 1600 and 1700  $\text{cm}^{-1}$ , is commonly used to determine the amide mode. The ATR-FTIR spectrum showed a strong amide I band around 1630  $\text{cm}^{-1}$  and a weak band around 1675  $\text{cm}^{-1}$ , indicating that an antiparallel  $\beta$ -sheet conformation was predominant [25], suggesting that even such a small fragment peptide ( $j$ ) preferably formed  $\beta$ -sheet conformation as seen for RU006 and RU065 ( $a$ , [Ant<sup>6</sup>]-RU006) in the literature [25]. This presumably contributed to the enrichment of gold ions during self-assembly and the densification of the obtained metallic gold-peptide composites resulting in easy separation [27].

Interestingly, peptides RU065<sub>4-8</sub> (*j*) and RU065<sub>3-7</sub> (*o*), each of which comprised five amino acids, showed very different Au/Pt atomic ratios even though the only difference was that the Ile residue in RU065<sub>4-8</sub> (*j*) was replaced with an Ala residue in RU065<sub>3-7</sub> (*o*). Further, peptides RU065<sub>4-8</sub> (*j*) and RU065<sub>5-7</sub> (*q*) had similar hydrophathy characteristics but different numbers of amino acid residues, and also showed a significant difference in ratios. These variations can presumably be ascribed to the important role of amide moieties in forming the hydrogen bond networks that facilitated peptide self-assembly and metal precipitation. These results strongly suggest that adequate hydrophobicity and the presence of several amide moieties are important to the self-assembly process that, in turn, accommodates and concentrates gold ions with the subsequent reduction of these ions within the assemblies to provide high Au/Pt atomic ratios.

**Transmission Electron Microscopy and X-ray Diffraction.** The precipitates generated from mixtures of RU065<sub>4-8</sub> (*j*) with H<sub>2</sub>HAuCl<sub>4</sub> and H<sub>2</sub>PtCl<sub>6</sub> were characterized using TEM (Figure 5A–C). The image in Figure 5A demonstrates a spherical particle with a diameter of approximately 30 nm along with numerous other spherical particles with diameters on the order of 2 nm. The image in Figure 5B presents a magnified view of the nanosphere surrounded by the yellow square in Figure 5A. This image indicates a *d*-spacing of 2.35 Å that corresponds to the Au<111> direction in crystals having a face-centered cubic (fcc) structure [27,36]. A magnified view of the region within the blue square is provided in Figure 5C, with a *d*-spacing of 2.21 Å that equates to the Pt<111> direction in an fcc crystal [27,36]. These results were verified by acquiring X-ray diffraction (XRD) data. The powder XRD pattern in Figure 5D contains four broad peaks at 2θ values of 38.2°, 44.4°, 64.6°, and 77.6° that are attributed to (111), (200), (220), and (311) crystal planes, respectively, in metallic gold having an fcc crystal structure. XRD peaks corresponding to elemental platinum (2θ = 39.8°, 46.3°, and 67.5°, assigned to (111), (200) and (220) crystal planes, respectively) were not observed, likely because the platinum nanospheres had crystallite sizes smaller than those detectable by powder XRD. These results suggest that the precipitates from the reaction of RU065<sub>4-8</sub> (*j*), H<sub>2</sub>HAuCl<sub>4</sub>, and H<sub>2</sub>PtCl<sub>6</sub> were in a metallic state and that metallic platinum formed much smaller particles than metallic gold.

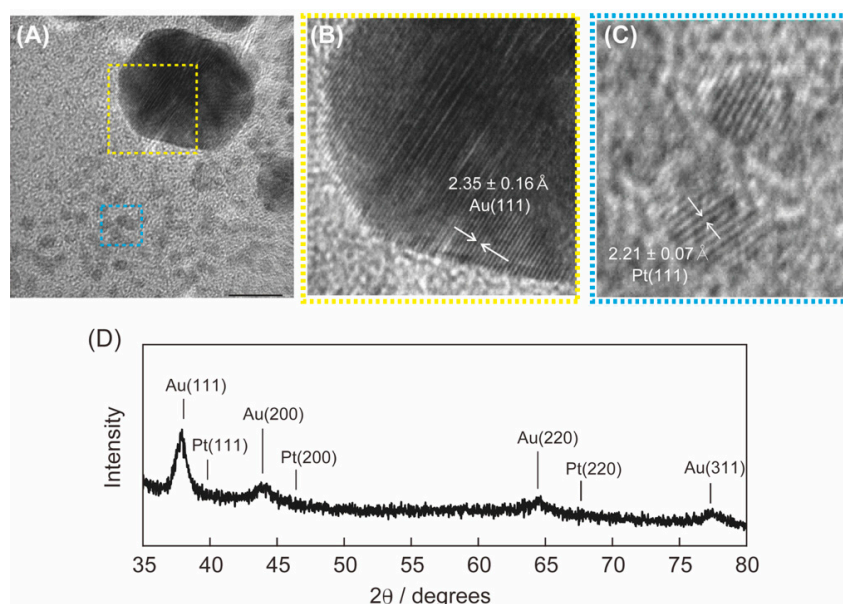


**Figure 5.** (A) TEM image of precipitate obtained from mixture of H<sub>2</sub>HAuCl<sub>4</sub>, H<sub>2</sub>PtCl<sub>6</sub>, and RU065<sub>4-8</sub> (*j*) (scale bar = 10 nm). Expanded TEM images of the areas surrounded by (B) yellow and (C) blue squares in panel A. (D) X-ray diffraction pattern for precipitate from mixture of H<sub>2</sub>HAuCl<sub>4</sub>, H<sub>2</sub>PtCl<sub>6</sub>, and RU065<sub>4-8</sub> (*j*). Diffraction peaks were assigned based on JCPDS data for face-centered cubic (fcc) structures for each element. Peptide = 2.0 × 10<sup>−4</sup> M, H<sub>2</sub>HAuCl<sub>4</sub> = H<sub>2</sub>PtCl<sub>6</sub> = 5.0 × 10<sup>−5</sup> M in water. Reactions were conducted at 40 °C for 24 h in the dark.

**Gold Selectivity Assessment by ICP-OES.** ICP-OES was used to better assess the precise selectivity of the peptide-based recovery system for gold by quantifying residual ion concentrations in the supernatants obtained after centrifugation of mixtures comprising the peptides,  $\text{HAuCl}_4$  and  $\text{H}_2\text{PtCl}_6$  (Figure 6) [27,37]. As shown in Figure 6A, ICP-OES analyses of the supernatants of the reaction mixtures containing the original RU065 (*a*) revealed a residual Au(III)/Au(I) concentration of  $2.7 \times 10^{-6}$  M (equivalent to 95% recovery) and a residual Pt(IV)/Pt(II) concentration of  $3.7 \times 10^{-5}$  M (26% recovery). These results are comparable to those in our previous work [27].

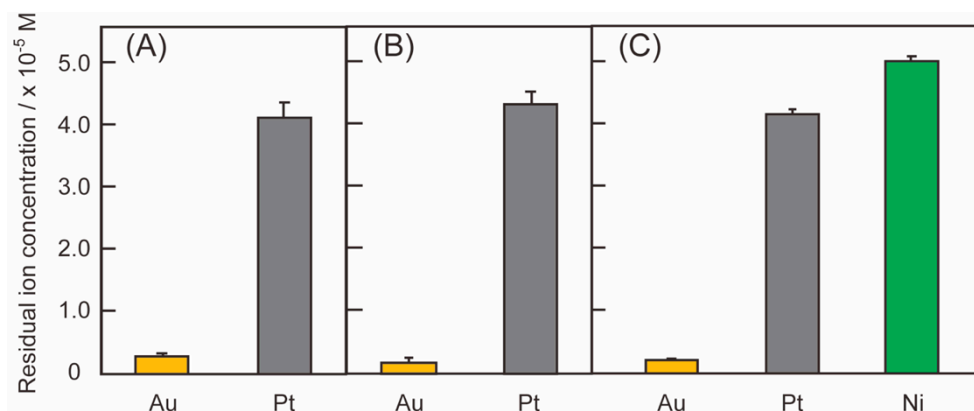


**Figure 6.** Quantification of residual Au, Pt, and Ni concentrations in supernatants from mixtures of  $\text{HAuCl}_4$  and  $\text{H}_2\text{PtCl}_6$  (and  $\text{Ni}(\text{NO}_3)_2$  for panel C) with (A) original RU065 (*a*) and (B,C) RU065<sub>4-8</sub> (*j*), as determined by ICP-OES analysis (mean  $\pm$  SD,  $n = 3$ ). Peptide =  $2.0 \times 10^{-4}$  M,  $\text{HAuCl}_4 = \text{H}_2\text{PtCl}_6 = \text{Ni}(\text{NO}_3)_2 = 5.0 \times 10^{-5}$  M in water. Reactions were conducted at 40 °C for 24 h in the dark.

ICP-OES analysis of the reaction mixtures containing RU065<sub>4-8</sub> (*j*) gave residual concentrations of  $1.6 \times 10^{-6}$  M (97% recovery) for Au(III)/Au(I) and  $3.9 \times 10^{-5}$  M (22% recovery) for Pt(IV)/Pt(II) in Figure 6B. The results for RU065 (*a*) and RU065<sub>4-8</sub> (*j*) were similar, suggesting that the latter has the same potential to selectively reduce/recover gold ions as RU065 (*a*), even though it has four fewer amino acids. Consequently, the minimum requirement for the structure would be Ac-Lys-Ala-Ant-Lys-Ile-NH<sub>2</sub>. The high recovery yields for gold with RU065 (*a*) and RU065<sub>4-8</sub> (*j*) suggest that RU065<sub>4-8</sub> (*j*) also concentrated gold ions on the basis of a mechanism involving self-assembly, reduction of gold ions to the metallic state and concentration, enabling easy separation of the metallic solids by simple centrifugation, as RU065 (*a*) did in our previous work [27]. However, the selectivity (that is, the Au recovery %/Pt recovery %) determined by ICP-OES was somewhat lower than the Au/Pt atomic ratio obtained from the EDS-FESEM analyses, as shown in Figure 2A. These small differences between the selectivity determined by ICP-OES and EDS-FESEM could be attributed to the formation of platinum nanoclusters that were difficult to separate by centrifugation (as shown in Figure 5A,C), such that different amounts of gold were determined using the two methods.

We next demonstrated selective gold reduction/recovery from a mixture of gold, platinum, and nickel ions using RU065<sub>4-8</sub> (*j*) to examine the effects of a transition metal. Figure 6C shows the residual ion concentrations in the supernatant obtained from a mixture of RU065<sub>4-8</sub> (*j*,  $2.0 \times 10^{-4}$  M),  $\text{HAuCl}_4$ ,  $\text{H}_2\text{PtCl}_6$ , and  $\text{Ni}(\text{NO}_3)_2$  (metal ion =  $5.0 \times 10^{-5}$  M each) in water. The data show residual concentrations of  $1.8 \times 10^{-6}$  M (96% recovery) for Au(III)/Au(I),  $4.1 \times 10^{-5}$  M (18% recovery) for Pt(IV)/Pt(II) and  $5.0 (4.96) \times 10^{-5}$  M (approximately 1% recovery) for Ni(II). These results suggest that positively charged transition metal ions such as nickel were more difficult to reduce than noble metals and so primarily remained in solution as a consequence of charge repulsion between the Ni(II) ions and RU065<sub>4-8</sub> (*j*). Therefore, the present peptide-based system could be robust for selective gold recovery from a mixture of base metal ions with redox potentials lower than those for noble metal ions.

As reported by Kim et al., a tannin-TiO<sub>2</sub> heterostructure selectively adsorbed gold ions from a solution containing nine different metal ions ([metal ion] =  $1.0 \times 10^{-3}$  M each) with an Au/Pt ratio of ca. 50 under light irradiation [38]. Dogan et al. showed that nitrile and amidoxime-containing nanoporous polymer microspheres adsorbed gold ions from a solution containing eleven different metal ions ([metal ion] = 100 ppb each) with an Au/Pt ratio of ca. 3.8 [39]. These results suggest that for high metal ion concentrations, an excellent Au/Pt ratio can be achieved, whereas for low metal ion concentrations, it is difficult to improve the gold selectivity against platinum. Thus, our results (metal ion =  $5.0 \times 10^{-5}$  M each) are competitive and it is possible to design low-cost gold-selective recovery agents based on the active short peptide RU065<sub>4-8</sub> (*j*).

**Mechanistic Study.** Our prior work demonstrated that the original RU065 (*a*) was able to generate metal nanocrystals after a span of 4 h. This was a more rapid process than was evident using another peptide incorporating a naphthalene moiety in place of an anthracene ring. Specifically, EDS-FESEM indicated that a combination of RU065 (*a*), HAuCl<sub>4</sub>, and H<sub>2</sub>PtCl<sub>6</sub> decreased the Au/Pt ratio from 12.3 to 7.3 after 4 h. On this basis, we suggest that gold nanocrystals were initially generated as the HAuCl<sub>4</sub> was reduced by the anthracene rings, while nanocrystals of platinum were formed more gradually. Consequently, Au(III) was rapidly changed to metallic gold with limited formation of Au(I) as an intermediate, while Pt(IV)/Pt(II) ions received electrons less slowly to produce a platinum precipitate [27–29].

The present work also attempted to elucidate the mechanism of the selective reduction/recovery of metallic gold from the mixture of HAuCl<sub>4</sub> and H<sub>2</sub>PtCl<sub>6</sub> by RU065<sub>4-8</sub> (*j*). This was done by analyzing sample solutions using MALDI-TOFMS. Figure 7A shows the MALDI-TOFMS profile for the solution containing RU065<sub>4-8</sub> (*j*) prepared using the standard conditions described in the Experimental Section but without HAuCl<sub>4</sub> and H<sub>2</sub>PtCl<sub>6</sub>. A single peak was obtained at  $m/z = 748.5$ , corresponding to the molecular ion peak (that is, [M + H]<sup>+</sup>) along with a less intense peak at  $m/z = 770$  likely corresponding to [M + Na]<sup>+</sup>. These data indicate that RU065<sub>4-8</sub> (*j*) remained intact after a 24 h incubation in water at 40 °C. In contrast, the MALDI-TOFMS profile for the sample solution prepared under the standard conditions contained peaks at  $m/z = 748.7$  and  $770.9$  corresponding to [M + H]<sup>+</sup> and [M + Na]<sup>+</sup> for the intact RU065<sub>4-8</sub> (*j*) but also at  $m/z = 764.8$ ,  $779.0$ ,  $802.9$ , and  $818.1$ , corresponding to [M + O + H]<sup>+</sup>, [M + 2O + H]<sup>+</sup>, [M + 2O + Na]<sup>+</sup>, and [M + 2O + K]<sup>+</sup>, and peaks around  $m/z = 767$  likely attributable to [M + K]<sup>+</sup> and/or [M + O + Na]<sup>+</sup> (Figure 7B,C). These results strongly suggest that the anthracene rings were oxidized by gold and/or platinum ions to generate ketone, hydroxide, quinone, and/or hydroquinone-like functional groups during the self-assembly of the peptides and the subsequent reduction of the metal ions to form gold-rich metallic precipitates [40]. However, since only limited reaction kinetics data were obtained in our previous study [27], further experiments are required to clarify the reaction mechanisms that lead to good gold selectivity.

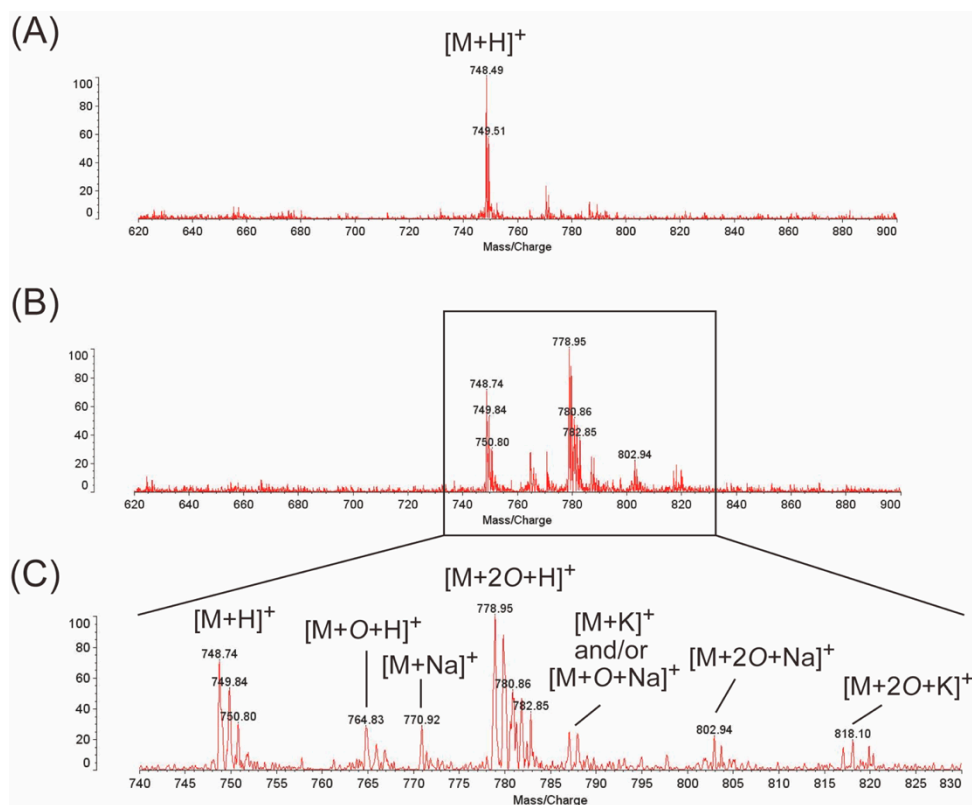


**Figure 7.** MALDI-TOFMS data obtained from (A) RU065<sub>4-8</sub> (*j*) only, (B) mixture of HAuCl<sub>4</sub>, H<sub>2</sub>PtCl<sub>6</sub>, and RU065<sub>4-8</sub> (*j*), and (C) expanded region of mass spectrum in panel B. The symbols 'O' in the labels indicates an oxygen atom added to the anthracene ring of RU065<sub>4-8</sub> (*j*). Peptide =  $2.0 \times 10^{-4}$  M, HAuCl<sub>4</sub> = H<sub>2</sub>PtCl<sub>6</sub> =  $5.0 \times 10^{-5}$  M in water. Each reaction was conducted at 40 °C for 24 h in the dark.

#### 4. Conclusions

The anthracene-containing peptide RU065 (*a*) and its fragment peptides (*b-x*) were synthesized and investigated with regard to the selective metallic recovery of gold. These trials used peptides ( $2.0 \times 10^{-4}$  M each) in homogenous aqueous solutions containing dilute HAuCl<sub>4</sub> and H<sub>2</sub>PtCl<sub>6</sub> ( $5.0 \times 10^{-5}$  M each) to determine the minimum required structural composition. Ten peptides provided suitable Au/Pt atomic ratios on the order of 8 based on the data obtained from EDS-FESEM and HPLC analyses. The smallest useable peptide structure was determined to be RU065<sub>4-8</sub> (*j*), a fragment peptide made of five amino acid residues (an Ant, two Lys, one Ile, and one Ala). Therefore, an anthracene ring accompanied by residues providing adequate hydrophobicity, two positive charges, and several amide groups are required to facilitate selective metallic gold precipitation/recovery. This process results in the subsequent oxygenation of the anthracene rings as determined by MALDI-TOFMS. We also demonstrated peptide-based selective gold recovery from a mixture containing gold, platinum, and nickel ions using the RU065<sub>4-8</sub> (*j*) fragment. This system successfully precipitated and recovered metallic gold by simple centrifugation with high selectivity and good recovery, as indicated by ICP-OES data. We believe that the minimum structural features for miniaturized active molecules as demonstrated herein will assist in the future design of small, non-peptidyl anthracene derivatives that selectively precipitate/recover metallic gold with a high gold recovery rate per unit mass of recovery agents. This could allow the development of a low-cost, one-pot gold recovery system applicable on a large scale.

**Supplementary Materials:** The following are available online at <https://www.mdpi.com/article/10.3390/pr9112010/s1>, Molecular structures (Figure S1), MALDI-TOFMS and HPLC data (Tables

S1 and S2, Figure S2), UV–Vis absorption spectra (Figure S3), EDS–FESEM elemental distribution images and corresponding EDS spectra for all peptides (*a–x*) (Figure S4).

**Author Contributions:** Conceptualization, K.-y.T. and M.A.; methodology, K.-y.T. and M.A.; investigation, K.-y.T., T.T., S.T., H.O. and M.A.; data curation, T.T., S.T., H.O. and T.I.; writing—original draft preparation, K.-y.T.; writing—review and editing, K.-y.T. and M.A.; supervision, K.-y.T. and M.A.; project administration, K.-y.T.; funding acquisition, K.-y.T. All authors have read and agreed to the published version of the manuscript.

**Funding:** This study was supported in part by the Ryukoku University Science and Technology Funds 2018 and by a JSPS KAKENHI grant (no. JP20K05713).

**Institutional Review Board Statement:** Not applicable.

**Informed Consent Statement:** Not applicable.

**Data Availability Statement:** Not applicable.

**Acknowledgments:** Electron microscopy images were obtained at the Ryukoku University Electron Microscope Laboratory.

**Conflicts of Interest:** The authors declare no conflict of interest.

## Abbreviations

Ala: L-alanine; Ant: L-2-anthrylalanine; ATR-FTIR: attenuated total reflection Fourier transform Infrared; Boc: *t*-butyloxycarbonyl; DIEA: *N,N*-diisopropylethylamine; EDS-FESEM: energy dispersive X-ray spectroscopy-field emission scanning electron microscopy; Fmoc: 9-fluorenylmethoxycarbonyl; HBTU: 2-(1*H*-benzotriazole-1-yl)-1,1,3,3-tetramethyluronium hexafluorophosphate; HOBt·H<sub>2</sub>O: 1-hydroxybenzotriazole monohydrate; HPLC: high performance liquid chromatography; ICP-OES: inductively coupled plasma-optical emission spectroscopy; Ile: L-isoleucine; Lys: L-lysine; MALDI-TOFMS: matrix-assisted laser desorption/ionization time-of-flight mass spectrometry; Nal: L-2-naphthylalanine; NMP: *N*-methylpyrrolidone; PPD: piperidine; TEM: transmission electron microscopy; TFA: trifluoroacetic acid; TFE: 2,2,2-trifluoroethanol; XRD: X-ray diffraction.

## References

1. Kaya, M. Recovery of Materials and Nonmaterials from Electronic Wastes by Physical and Chemical Recycling Processes. *Waste Manag.* **2016**, *57*, 64–90. [[CrossRef](#)]
2. Kim, J.; Kim, K.R.; Hong, Y.; Choi, S.; Yavuz, C.T.; Kim, J.W.; Nam, Y.S. Photochemically Enhanced Selective Adsorption of Gold Ions on Tannin-Coated Poros Polymer Microspheres. *ACS Appl. Mater. Interfaces* **2019**, *11*, 21915–21925. [[CrossRef](#)] [[PubMed](#)]
3. Cox, M. Solvent Extraction in Hydrometallurgy. In *Solvent Extraction Principles and Practice, Second Edition, Revised and Expanded*; Rydberg, J., Cox, M., Musikas, C., Choppin, G.R., Eds.; Marcel Dekker, Inc.: New York, NY, USA, 2004; pp. 455–505.
4. Won, S.W.; Kotte, P.; Wei, W.; Lim, A.; Yum, Y.S. Biosorbents for Recovery of Precious Metals. *Biosens. Technol.* **2014**, *160*, 203–212. [[CrossRef](#)] [[PubMed](#)]
5. Syed, S. Recovery of Gold from Secondary Sources—A Review. *Hydrometallurgy* **2012**, *115–116*, 30–51. [[CrossRef](#)]
6. Wiecka, Z.; Rzelewska-Piekut, M.; Wojciechowska, I.; Wieszczycka, K.; Regel-Rosocka, M. Recovery of Palladium(II) and Platinum(IV) in Novel Extraction Systems. *Materials* **2021**, *14*, 285. [[CrossRef](#)]
7. Yamada, M.; Rajiv Gandhi, M.; Shibayama, A. Rapid and Selective Recovery of Palladium from Platinum Group Metals and Base Metals Using a Thioamide-Modified Calix[4]arene Extractant in Environmentally Friendly Hydrocarbon Fluids. *Sci. Rep.* **2018**, *8*, 16909. [[CrossRef](#)]
8. Lanaridi, O.; Sahoo, A.R.; Limbeck, A.; Naghdi, S.; Eder, D.; Eitenberger, E.; Csendes, Z.; Schnüürch, M.; Bica-Schröder, K. Toward the Recovery of Platinum Group Metals from a Spent Automotive Catalyst with Supported Ionic Liquid Phases. *ACS Sustain. Chem.* **2021**, *9*, 375–386. [[CrossRef](#)]
9. Chen, Z.; Wang, D.; Feng, S.; Liu, H. An Imidazole Thione-Modified Polyhedral Oligomeric Silsesquioxane for Selective Detection and Adsorptive Recovery of Au(III) from Aqueous Solutions. *ACS Appl. Mater. Interfaces* **2021**, *13*, 23592–23605. [[CrossRef](#)]
10. Kasper, A.C.; Carrillo Abad, J.; García Gabaldón, M.; Veit, H.M.; Pérez Herranz, V. Determination of the Potential Gold Electrowinning from an Ammoniacal Thiosulphate Solution Applied to Recycling of Printed Circuit Board Scraps. *Waste Manag. Res.* **2016**, *34*, 47–57. [[CrossRef](#)]
11. Fogarasi, S.; Imre-Lucaci, F.; Imre-Lucaci, Á.; Ilea, P. Copper Recovery and Gold Enrichment from Waste Printed Circuit Boards by Mediated Electrochemical Oxidation. *J. Hazard. Mater.* **2014**, *273*, 215–221. [[CrossRef](#)]

12. Ronka, S. New sulfur-containing polymeric sorbents based on 2,2'-thiobisethanol dimethacrylate. *Pure Appl. Chem.* **2019**, *91*, 409–420. [[CrossRef](#)]
13. Ronka, S.; Targońska, S. Gold(III) ions sorption on sulfur-containing polymeric sorbent based on 2,2'-thiobisethanol dimethacrylate. *Sep. Sci. Technol.* **2020**, *55*, 2158–2169. [[CrossRef](#)]
14. Negrea, A.; Ronka, S.; Ciopec, M.; Duteanu, N.; Negrea, P.; Mihailescu, M. Kinetics, Thermodynamics and Equilibrium Studies for Gold Recovery from Diluted Waste Solution. *Materials* **2021**, *14*, 5325. [[CrossRef](#)]
15. Wu, X.; Lin, H.; Dai, F.; Hu, R.; Tang, B.Z. Functional Polyselenoureas for Selective Gold Recovery Prepared from Catalyst-Free Multicomponent Polymerizations of Elemental Selenium. *CCS Chem.* **2020**, *2*, 191–202. [[CrossRef](#)]
16. Daniel, M.-C.; Astruc, D. Gold Nanoparticles: Assembly, Supramolecular Chemistry, Quantum-Size-Related Properties, and Applications toward Biology, Catalysis, and Nanotechnology. *Chem. Rev.* **2004**, *104*, 293–346. [[CrossRef](#)]
17. Eustis, S.; El-Sayed, M.A. Why Gold Nanoparticles Are More Precious than Pretty Gold: Noble Metal Surface Plasmon Resonance and Its Enhancement of the Radiative and Nonradiative Properties of Nanocrystals of Different Shapes. *Chem. Soc. Rev.* **2006**, *35*, 209–217. [[CrossRef](#)] [[PubMed](#)]
18. Hu, M.; Chen, J.; Li, Z.-Y.; Au, L.; Hartland, G.V.; Li, X.; Marquez, M.; Xia, Y. Gold Nanostructures: Engineering Their Plasmonic Properties for Biomedical Applications. *Chem. Soc. Rev.* **2006**, *35*, 1084–1094. [[CrossRef](#)]
19. Cobley, C.M.; Chen, J.; Cho, E.C.; Wang, L.V.; Xia, Y. Gold Nanostructures: A Class of Multifunctional Materials for Biomedical Applications. *Chem. Soc. Rev.* **2011**, *40*, 44–56. [[CrossRef](#)]
20. Ghosh, S.K.; Pal, T. Interparticle Coupling Effect on the Surface Plasmon Resonance of Gold Nanoparticles: From Theory to Applications. *Chem. Rev.* **2007**, *107*, 4797–4862. [[CrossRef](#)]
21. Jain, P.K.; Huang, X.; El-Sayed, I.H.; El-Sayed, M.A. Noble Metals on the Nanoscale: Optical and Photothermal Properties and Some Applications in Imaging, Sensing, Biology, and Medicine. *Acc. Chem. Res.* **2008**, *41*, 1578–1586. [[CrossRef](#)]
22. Murphy, C.J.; Gole, A.M.; Stone, J.W.; Sisco, P.N.; Alkilany, A.M.; Goldsmith, E.C.; Baxter, S.C. Gold Nanoparticles in Biology: Beyond Toxicity to Cellular Imaging. *Acc. Chem. Res.* **2008**, *41*, 1721–1730. [[CrossRef](#)] [[PubMed](#)]
23. Sperling, R.A.; Gil, P.R.; Zhang, F.; Zanella, M.; Parak, W.J. Biological Applications of Gold Nanoparticles. *Chem. Soc. Rev.* **2008**, *37*, 1896–1908. [[CrossRef](#)] [[PubMed](#)]
24. Boisselier, E.; Astruc, D. Gold Nanoparticles in Nanomedicine: Preparations, Imaging, Diagnostics, Therapies and Toxicity. *Chem. Soc. Rev.* **2009**, *38*, 1759–1782. [[CrossRef](#)]
25. Tomizaki, K.-Y.; Wakizaka, S.; Yamaguchi, Y.; Kobayashi, A.; Imai, T. Ultrathin Gold Nanoribbons Synthesized within the Interior Cavity of a Self-Assembled Peptide Nanoarchitecture. *Langmuir* **2014**, *30*, 846–856. [[CrossRef](#)] [[PubMed](#)]
26. Tomizaki, K.-Y.; Kishioka, K.; Kobayashi, H.; Kobayashi, A.; Yamada, N.; Kataoka, S.; Imai, T.; Kasuno, M. Roles of Aromatic Side Chains and Template Effects of the Hydrophobic Cavity of a Self-Assembled Peptide Nanoarchitecture for Anisotropic Growth of Gold Nanocrystals. *Bioorg. Med. Chem.* **2015**, *23*, 7282–7291. [[CrossRef](#)]
27. Tomizaki, K.-Y.; Okamoto, T.; Tonoda, T.; Imai, T.; Asano, M. Selective Gold Recovery from Homogenous Aqueous Solutions Containing Gold and Platinum Ions by Aromatic Amino Acid-Containing Peptides. *Int. J. Mol. Sci.* **2020**, *21*, 5060. [[CrossRef](#)]
28. Ataee-Esfahani, H.; Wang, L.; Nemoto, Y.; Yamauchi, Y. Synthesis of Bimetallic Au@Pt Nanoparticles with Au core and Nanostructured Pt Shell toward Highly Active Electrocatalysts. *Chem. Mater.* **2010**, *22*, 6310–6318. [[CrossRef](#)]
29. Guo, S.; Li, J.; Dong, S.; Wang, E. Three-Dimensional Pt-on-Au Bimetallic Dendritic nanoparticle: One-Step, High-Yield Synthesis and Its Bifunctional Plasmonic and Catalytic Properties. *J. Phys. Chem. C* **2010**, *114*, 15337–15342. [[CrossRef](#)]
30. Chan, W.C.; White, P.D. *Fmoc Solid Phase Peptide Synthesis: A Practical Approach*; Oxford University Press: New York, NY, USA, 2000; pp. 41–76.
31. Tomizaki, K.-Y.; Tanaka, A.; Shimada, H.; Nishizawa, K.; Wada, T.; Imai, T. The Alkyl Linkers in Tandem-Homodimers of a  $\beta$ -Sheet-Forming Nonapeptide Affect the Self-Assembled Nanostructures. *Bioorg. Med. Chem. Lett.* **2016**, *26*, 2659–2662. [[CrossRef](#)]
32. Liu, L.-P.; Deber, C.M. Guidelines for Membrane Protein Engineering Derived from De Novo Designed Model Peptides. *Biopolymers* **1998**, *47*, 41–62. [[CrossRef](#)]
33. Sethi, M.; Knecht, M.R. Understanding the Mechanism of Amino Acid-Based Au Nanoparticle Chain Formation. *Langmuir* **2010**, *26*, 9860–9874. [[CrossRef](#)]
34. Nguyen, M.A.; Hughes, Z.E.; Lin, Y.; Li, Y.; Swihart, M.T.; Knecht, M.R.; Walsh, T.R. Peptide-Mediated Growth and Dispersion of Au Nanoparticles in Water via Sequence Engineering. *J. Phys. Chem. C* **2018**, *122*, 11532–11542. [[CrossRef](#)]
35. Chen, X.; Yuan, B.; Yu, F.; Liu, Y.; Xie, C.; Yu, S. Hydrogenation of  $\alpha$ -Pinene over Platinum Nanoparticles Reduced and Stabilized by Sodium Lignosulfonate. *ACS Omega* **2020**, *5*, 8902–8911. [[CrossRef](#)] [[PubMed](#)]
36. Yan, J.; Pan, Y.; Cheetham, A.G.; Lin, Y.-A.; Wang, W.; Cui, H.; Liu, C.-J. One-Step Fabrication of Self-Assembled Peptide Thin Films with Highly Dispersed Noble Metal Nanoparticles. *Langmuir* **2013**, *29*, 16051–16057. [[CrossRef](#)]
37. Mladenova, E.; Karadjova, I.; Tsalev, D.L. Solid-phase Extraction in the Determination of Gold, Palladium, and Platinum. *J. Sep. Sci.* **2012**, *35*, 1249–1265. [[CrossRef](#)] [[PubMed](#)]
38. Kim, K.R.; Choi, S.; Yavuz, C.T.; Nam, Y.S. Direct Z-Scheme Tannin-TiO<sub>2</sub> Heterostructure for Photocatalytic Gold Ion Recovery from Electronic Waste. *ACS Sustain. Chem. Eng.* **2020**, *8*, 7359–7370. [[CrossRef](#)]

- 
39. Dogan, N.A.; Hong, Y.; Ozdemir, E.; Yavuz, C.T. Nanoporous Polymer Microspheres with Nitrile and Amidoxime Functionalities for Gas Capture and Precious Metal Recovery from E-Waste. *ACS Sustain. Chem. Eng.* **2019**, *7*, 123–128. [[CrossRef](#)]
  40. Clarke, C.; Tournay, J.; Johnson, K. Oxidation of Anthracene Using Waste Mn Oxide Minerals: The Importance of Wetting and Drying Sequences. *J. Hazard. Mater.* **2012**, *205–206*, 126–130. [[CrossRef](#)]